Singular perturbations and torsional wrinkling in a truncated hemispherical thin elastic shell

Ciprian D. Coman[1†] and Andrew P. Bassom[2‡]

[1] *Department of Computer Science, School of Computing & Engineering, University of Huddersfield, HD1 3DH, Huddersfield, UK*

[2] *School of Natural Sciences, University of Tasmania, Private Bag 37, Hobart TAS 7001, Australia*

March 26, 2022

Abstract

The work described in this paper is concerned with providing a rational asymptotic analysis for the partial wrinkling bifurcation of a thin elastic hemispherical segment in which the upper rim experiences in-plane circular shearing relative to the other circular edge. The mathematical structure of the associated complex-valued boundary eigenvalue problem is revealed by using the method of matched asymptotic expansions. Our key result is a three-term asymptotic formula for the critical load in terms of a suitable small parameter proportional to the ratio between the thickness and the radius of the shell. Comparisons of this formula with direct numerical simulations provide further insight into the range of validity of the results derived herein.

Keywords: partial wrinkling, boundary layers, DMV thin-shell theory, matched asymptotics.

[†] cdc3p@yahoo.com

[‡] andrew.bassom@utas.edu.au

1 Introduction

Spherical geometries have played a pivotal role in the historical development of thin shell theory due to their unique symmetry properties and concomitant simplifications. For example, regarded as a three-dimensional surface, the sphere enjoys the remarkable property that its first and second fundamental tensors are proportional to each other, while the stress resultant and stress couple tensors used in mathematical models of thin spherical shells turn out to be symmetric by default (e.g., [33, 51]). It is thus not surprising that the governing linear equations describing the static equilibrium of thin spherical shells are amenable to closed-form solutions, notwithstanding their apparent complexity and the presence of variable coefficients. However, as these solutions involve hypergeometric equations with complex-valued coefficients (whose solutions are known to be very slowly convergent series [44]), a great deal of effort had gone into finding practical simplifications for the equations of thin spherical shells; two such distinct approaches emerged during the first half of the 20th century.

One of the general strategies can be traced back to the concept of the 'edge effect' (or 'boundary layer'); a term coined by H. Reissner [59] in connection to small *axisymmetric* deformation of spherical shells. This approach is usually referred to as 'asymptotic integration' in the thin-shell literature and it amounts to exploiting the presence of the ubiquitous parameter $0 < (h/R) \ll 1$ (see Figure 1) in order to derive WKB-type approximations for the corresponding thin-shell equations. Blumenthal [3, 4], Geckler [27, 28], and Hetényi [34] are some of the key names associated with fundamental developments in this area. The case of *non-axisymmetric* deformations in thin spherical shells was originally tackled by Havers [32] (see also Flügge's account in [24]), who also discovered that Blumenthal's earlier approach was still relevant to deformations lacking radial symmetry provided that some small mathematical adjustments were introduced. Building upon Havers' pioneering work as well as Langer's [39] ideas of uniformly valid asymptotic solutions for ordinary differential equations with transition/turning points (e.g., see [22]), much later Leckie [40, 41] provided a definitive treatment of WKB-type approximations valid for any spherical geometry and general loading conditions.

A second class of simplifications vis-á-vis spherical shells is based on restricting the scope of the general theory to certain spatial regions that are regarded as being *shallow*; for a precise definition of the *shallow-shell kinematic assumption* we refer to standard texts on thin-shell theory (e.g., [7, 31, 51, 69]). This is a far-reaching simplifying hypothesis that is equally applicable to both the nonlinear kinematics of general thin shells and the linear theory. In particular, it leads to tractable differential equations that are amenable to detailed theoretical investigations, especially in the context of pre-stressed configurations and buckling instabilities (e.g., [11, 17]). For the hemispherical geometry seen in Figure 1, the "shallow" regions correspond to the two shaded areas. The (dark orange) polar region defines what is typically known as a 'shallow spherical cap', a configuration that has been the subject of innumerable stability studies; the reader is directed to [17] and the references therein for pointers to some of the relevant literature. By contrast, the (yellow) equatorial strip shown in Figure 1 corresponds to a 'shallow truncated hemisphere' and has been far less investigated; it is this particular configuration that we are interested in. One of our aims is to explore the torsional buckling of such shallow spherical segments when their circular edges are subjected to uniformly distributed in-plane shearing forces (acting in opposite directions).

There are only a handful of studies in the literature that deal with circumferential shearing instabilities of hemispherical thin shells. Mow and Sadowski [47] carried out an early investigation into the buckling of an internally pressurised spherical shell twisted by two equilibrating torques applied by means of flanges at the poles of their hollow sphere. The critical buckling torque was calculated in an ad-hoc manner by employing a variational approach, with the basic state being described by the corresponding linear membrane solution. Experimental work reported by the same authors revealed

the *local* nature of the instability which took the form of a single "oblong-elliptic" dimple confined near each of the two flanges mentioned above; as the torque increased past its critical threshold it was also noticed that more dimples formed around the poles. In more recent times, Tall *et al.* [65] used commercially available FE software to compute interactive buckling curves for a full hemispherical shell under the combined action of both external pressure and circular shearing of the equatorial edge. They also examined the post-buckling behaviour when the pressure was absent and concluded that their configuration was less sensitive to geometrical imperfections than an externally pressurised shell; the buckling pattern itself consisted of a large number of regular oblique ripples situated near the equator, but this number was found to decrease in the far post-buckling regime. A further study related to the topic of our investigation was reported by Yinyi [72]. In that paper a novel set of bifurcation equations is employed in conjunction with a simple-minded Galerkin-type procedure to study torsional instabilities of non-shallow hemispherical shells under the action of tangential torsional loads, non-uniformly distributed over the lateral surface of the hemisphere. Unfortunately, given the scarcity of the details provided in [72] it is rather difficult to ascertain the validity of the buckling equations used.

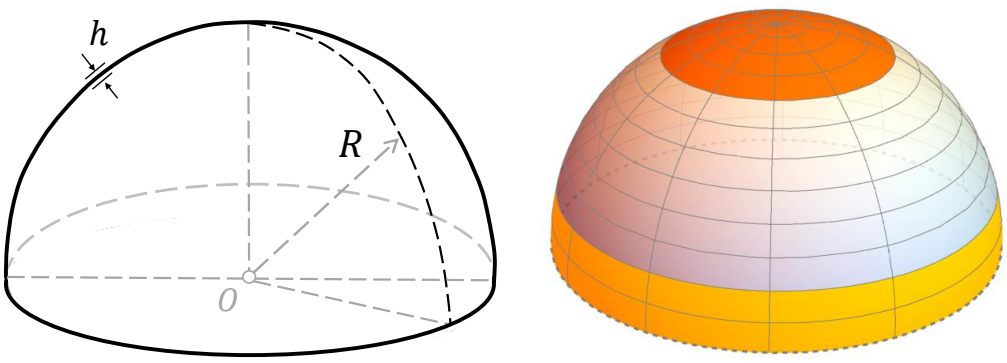

Figure 1: Hemispherical geometry. *Left:* the definitions of the parameters h (thickness) and R (radius) mentioned in the main text; *right:* the shaded areas correspond to the two regions that could be regarded as geometrically shallow.

With regard to further investigations involving truncated hemispherical thin shells, free-vibration problems seem to have attracted considerable interest [21, 42, 63, 50] due to their relevance in nuclear power plants, aviation and civil engineering [1, 29, 36, 73]. Spherical shells are also used in the oil and gas sector for storage purposes (e.g., as cargo containers for liquefied natural gas). Certain partially filled conditions can cause combined meridional tension and circumferential compression, eventually leading to an exotic form of localised buckling (e.g., see [53, 54, 61]). As shown recently by one of us [12], the asymptotic structure of that phenomenon can be explained by considering a truncated shallow hemispherical shell subjected to vertical tensile forces uniformly distributed along its circular rims (additional complementary information can be found in [6, 37, 71]). Other interesting researches dealing with buckling of shallow truncated hemispherical include those by Hutchinson [35] and Blum & McComb [2].

In this work we are motivated in extending a matched-asymptotics strategy [14] previously developed in connection to a flat annular plate for which the outer edge is uniformly stretched while

the inner rim undergoes in-plane rotation through a small angle. This is an archetypal configuration characterised by *partial wrinkling* (e.g., see [13, 46, 57]), i.e., the corresponding out-of-plane eigendeformations are localised near the inner hole rather than spreading across the entire span of the annulus. From a theoretical point of view the presence of torsional loads in rotationally symmetric geometries leads to a break in that symmetry. This has severe repercussions if a normal-mode approach is used to solve the corresponding linearised bifurcation equations; essentially, the number of equations doubles as one has to account for the amplitudes of both the 'sine' and the 'cosine' contributions in the assumed form of the normal-mode solution. As it will become clear in due course, despite such potential challenges, the asymptotic strategy of [14] proves to be robust enough to handle the torsional instabilities of our truncated hemisphere.

To better appreciate the philosophy of the approach taken in this work, it is perhaps worth emphasising a few general well-known facts about asymptotic approximations and linearised bifurcations (e.g., buckling). Typically, if the order of the corresponding bifurcation equations is $N \geq 2$, one aims to construct asymptotic approximations for a set of N linearly independent solutions (in terms of a suitably chosen large/small parameter). Expressing the general solution as a linear combination of the approximations just mentioned, and then applying the homogeneous boundary conditions results in an $(N \times N)$ determinantal equation that yields the critical value of the bifurcation parameter. If expanded, this determinant becomes just one typically complicated transcendental equation, which will still contain the original asymptotic parameter. One is then left with the task of solving this equation, either numerically or approximately, by using the methods of (say) reference [5]. This classical approach dates back to the 19th century and has been used extensively in the theory of hydrodynamic stability (e.g., see [43, 45]). More recently, Fu and his associates [25, 26], among others, have relied on the same approach to discuss a number of complicated buckling problems in Finite Elasticity. We should perhaps recall that the determinantal-equation approach has a number of shortcomings. For instance, it is inapplicable if the basic state is nonlinear and does not admit a closed-form expression; furthermore, if $N = 8$ (as in the case of thin-shell buckling) the expansion/simplification of the aforementioned determinant can often become too unwieldy to render useful practical information. An alternative to the route summarised above is based on Poincaré-type asymptotic expressions and is commonly used in the literature on dynamical systems (e.g., [8, 49]). In the language of matched asymptotic expansions [38], in this approach one constructs sequentially inner and outer expansions guided by the particular features of the problem at hand, thus circumventing the need to impose all boundary conditions simultaneously; nonlinearities and higher-dimensional problems pose no formal significant challenges as demonstrated in a number of our previous studies [11, 16, 17, 18, 19].

A somewhat more general scenario than the one presented in this paper was considered by Pogorelov [55] (pp. 165–171) based on purely geometrical arguments. His interest was in a cylindrical segment of a thin shell of revolution, in which one of the circular edges was twisted with respect to the other. With the help of a special variational principle and the theory of infinitesimal bendings of strictly convex surfaces, he derived a formula for the critical load, but there is no indication as to how one might improve that approximation. A very similar approach was used by the same author to study buckling of cylindrical shells under uniform pressure; we refer to Chapter 4 of [56] for an English account of that work. We also mention in passing that unlike the analysis reported in this paper, Pogorelov's study hinges on the use of *nonlinear* differential equations. Tovstik and Smirnov [66] used a WKB-type approach based on Olver's uniform expansion [52] (see also [22], pp. 168–170), in conjunction with the determinantal approach already mentioned, to work out approximations for the critical torsional buckling load in a situation similar to that considered by Pogorelov. The mathematical justification of the determinantal method is not trivial in this case because the shallow-shell equations employed have a transition/turning point. By writing the buckling problem as a first-order

system of ordinary differential equations, one can then take advantage of the specialised theory developed by Wasow [70] and Feschenko et. al [23]. Nevertheless, one is still left with evaluating an awkward (4×4) determinant. Since the authors of [66] do not include full details of their solution and show no comparisons with actual direct numerical simulations, it is difficult to gauge the accuracy of the approximation proposed therein.

With this background in mind, we proceed as follows. The coming section contains a succinct account of the main equations for the problem that forms the core of our study. Based on a suitable linearisation of the Donnell-Mushtari-Vlasov (DMV) shallow-shell theory specialised to spherical geometries, an eigenproblem governed by two coupled fourth-order partial differential equation is derived. These are further reduced to a novel singularly-perturbed system for two complicated ordinary differential equations with complex-valued variable coefficients. The asymptotic structure of this boundary eigenvalue problem is developed over the remaining sections. We start in §3 with a summary of a numerical investigation into the structure of the eigendeformations associated with the energy-minimum configurations of our system. In particular, these numerical results suggest that the buckling modes consist of a fast spatial oscillation modulated on a large scale by a boundary-layer type envelope. The insight gained from this preliminary study proves useful in guiding us through the formal calculations in §4, where the main asymptotic structure is captured by a non-trivial extension of the arguments developed in [12, 13]. As it happens, we find that the two-term approximation for the critical buckling load that follows from the analysis of §4 overshoots slightly the corresponding values obtained by direct numerical simulations of the full eigenproblem. This opens up the question as to what is the effect of later terms in our approximation vis-à-vis the issue just mentioned, and the rest of the paper is an attempt to investigate this. In §5 we augment the initial asymptotic analysis with the details of a thinner boundary layer needed to satisfy the derivative constraints associated with the flexurally clamped edges of our truncated hemisphere. The matching between the two boundary layers, as well as some higher-order calculations of the main asymptotic structure are further discussed in §6 and §7, which also include a suite of comparisons between the analytical predictions and direct numerical simulations. We conclude in §8 with a summary and a brief discussion.

2 The key equations

We consider a truncated hemispherical thin shell of radius R and uniform thickness h $(0 < h/R \ll 1)$ stressed by twisting one edge with respect to the other, the axis of the applied torque being perpendicular to the two horizontal bases of the hemisphere. We suppose that the torque is proportional to $M > 0$ and, for simplicity, in what follows it will be assumed that both edges of the shell are free to undergo in-plane rotations, but they are restrained from moving radially and undergoing transverse rotations; we refer to [6, 62] which provide further details on the practical realisation of such constraints. In spherical polar coordinates the geometry of our hemisphere is described with the help of the two angles ϕ and θ that have the meaning indicated in Figure 2 (note in particular that here ϕ is the *latitude* rather than the usual *co-latitude angle* more widely used in similar contexts). In addition, the shell is assumed to be made of an isotropic elastic material characterised by a Young's modulus $E > 0$ with Poisson's ratio $0 < \nu < 1/2$.

The bifurcation problem studied in this paper is based on the general DMV buckling equations for thin shells of revolution [7, 67, 68]. Using a system of curvilinear coordinates (α, β) which coincides with the orthogonal lines of principal curvature of the undeformed shell mid-surface, these equations

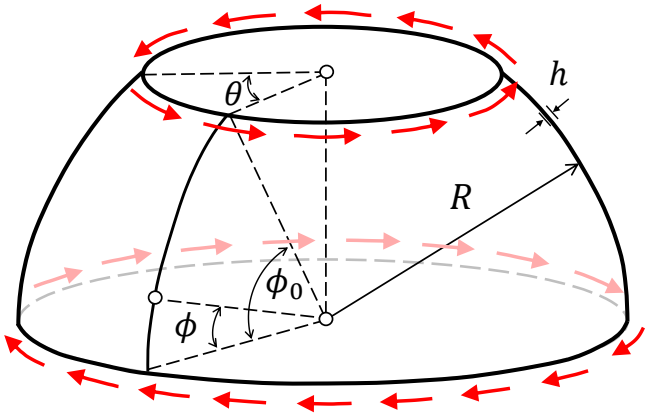

Figure 2: The geometry of the truncated hemispherical shell considered in the main text. Its mid-surface has radius $R > 0$ and it is parametrised by the spherical polar coordinates $0 \leq \phi \leq \phi_0 \ll \pi/2$ and $0 \leq \theta < 2\pi$.

can be expressed in the compact form (e.g., [31, 48])

$$\begin{cases} D\nabla^4 w - \nabla_t^2 w - \nabla_\kappa^2 \Phi = 0\,, & \text{(2.1a)} \\ (Eh)^{-1}\nabla^4 \Phi + \nabla_\kappa^2 w = 0\,, & \text{(2.1b)} \end{cases}$$

where $w \equiv w(\alpha, \beta)$ is the radial displacement and $\Phi \equiv \Phi(\alpha, \beta)$ corresponds to a stress function for the in-plane (or membrane) forces. The constant $D := Eh^3/12(1-\nu^2)$ denotes the usual bending rigidity of a thin shell, while the definitions of the various differential operators that feature in (2.1a) are given for the sake of completeness so

$$\nabla^2(\dots) \equiv \frac{1}{g_\alpha g_\beta}\left\{\frac{\partial}{\partial\alpha}\left[\frac{g_\beta}{g_\alpha}\frac{\partial}{\partial\alpha}(\dots)\right] + \frac{\partial}{\partial\beta}\left[\frac{g_\alpha}{g_\beta}\frac{\partial}{\partial\beta}(\dots)\right]\right\}, \qquad \nabla^4(\dots) \equiv \nabla^2\left[\nabla^2(\dots)\right], \tag{2.2a}$$

$$\nabla_\kappa^2(\dots) \equiv \frac{1}{g_\alpha g_\beta}\left\{\frac{\partial}{\partial\alpha}\left[\frac{1}{R_\beta}\frac{g_\beta}{g_\alpha}\frac{\partial}{\partial\alpha}(\dots)\right] + \frac{\partial}{\partial\beta}\left[\frac{1}{R_\alpha}\frac{g_\alpha}{g_\beta}\frac{\partial}{\partial\beta}(\dots)\right]\right\}, \tag{2.2b}$$

and

$$\nabla_t^2 w \equiv \frac{1}{g_\alpha g_\beta}\left\{\frac{\partial}{\partial\alpha}\left[\mathring{T}_\alpha\left(\frac{g_\beta}{g_\alpha}\right)\frac{\partial w}{\partial\alpha}\right] + \frac{\partial}{\partial\beta}\left[\mathring{T}_\beta\left(\frac{g_\alpha}{g_\beta}\right)\frac{\partial w}{\partial\beta}\right] + \frac{\partial}{\partial\alpha}\left(\mathring{S}\,\frac{\partial w}{\partial\beta}\right) + \frac{\partial}{\partial\beta}\left(\mathring{S}\,\frac{\partial w}{\partial\alpha}\right)\right\}. \tag{2.3}$$

In these expressions, g_α, g_β are the non-zero coefficients of the metric tensor on the undeformed mid-surface, R_α and R_β represent the principal radii of curvature, while $\mathring{T}_\alpha$, $\mathring{T}_\beta$, and $\mathring{S}$ correspond to the membrane stresses associated with the axisymmetric pre-buckling state of stress experienced by the truncated hemisphere.

For a spherical geometry $\alpha \to \phi$ and $\beta \to \theta$, so that $g_\phi = R$ and $g_\theta = R\cos\phi$. This allows us to calculate explicitly the expressions of the differential operators in (2.2) and (2.3), e.g.,

$$\nabla_\kappa^2 = R^{-3}\nabla_*^2\,, \qquad \nabla_*^2 \equiv R^2\nabla^2 = \frac{\partial^2}{\partial\phi^2} - \tan\phi\,\frac{\partial}{\partial\phi} + \sec^2\phi\,\frac{\partial^2}{\partial\theta^2}\,,$$

$$\nabla^4 = R^{-4}\nabla_*^4 \equiv R^{-4}\nabla_*^2\nabla_*^2\,.$$

Furthermore, for a spherical shell the pre-buckling state of stress is given by

$$\mathring{T}_\phi = \mathring{T}_\theta \equiv 0\,, \qquad \mathring{S} \equiv \mathring{S}(\phi) = \left(\frac{M}{2\pi R^2}\right)\sec^2\phi\,. \tag{2.4}$$

Next, by introducing the non-dimensional quantities

$$\widehat{w} := \frac{w}{R}\,, \qquad \widehat{\Phi} := \frac{\Phi}{EhR^2}\,, \qquad \mu := \sqrt{12(1-\nu^2)}\left(\frac{R}{h}\right)\,, \qquad \lambda := \frac{M\mu^2}{\pi R^2 Eh}\,, \tag{2.5}$$

the bifurcation system (2.1a) can be cast in the simplified form

$$\begin{cases} \nabla_*^4\widehat{w} - \mu^2\,\nabla_*^2\widehat{\Phi} + \lambda\,\mathcal{L}(\widehat{w}) = 0\,, & \text{(2.6a)} \\ \nabla_*^4\widehat{\Phi} + \nabla_*^2\widehat{w} = 0\,, & \text{(2.6b)} \end{cases}$$

where we have introduced the differential operator

$$\mathcal{L}(\dots) \equiv \sec^3\phi\,\left[\frac{\partial^2}{\partial\phi\partial\theta}(\dots) + \tan\phi\,\frac{\partial}{\partial\theta}(\dots)\right]\,.$$

Solutions of the coupled equations (2.6a) and (2.6b) are sought by looking for functions with separable variables. To this end, we write

$$\widehat{w}(\phi,\theta) = \mathfrak{Re}\left\{W(\phi)\mathrm{e}^{\mathrm{i}m\theta}\right\}\,, \qquad \widehat{\Phi}(\phi,\theta) = \mathfrak{Re}\left\{F(\phi)\mathrm{e}^{\mathrm{i}m\theta}\right\}\,, \tag{2.7a}$$

$$W(\phi) := W_{\mathrm{R}}(\phi) + \mathrm{i}W_{\mathrm{I}}(\phi)\,, \qquad F(\phi) := F_{\mathrm{R}}(\phi) + \mathrm{i}F_{\mathrm{I}}(\phi)\,, \qquad (\mathrm{i} = \sqrt{-1})\,, \tag{2.7b}$$

where the notation $\mathfrak{Re}(z)$ stands for the real part of $z \in \mathbb{C}$, and the "amplitude" functions $W_j(\phi)$, $F_j(\phi)$, $j \in \{\mathrm{R},\mathrm{I}\}$ are all real-valued. As explained shortly, the arbitrary integer $m \geq 0$ will be determined by the requirement that it should render the global minimum of the curve $\lambda = \lambda(m)$.

Performing the requisite calculations it turns out that the unknown complex amplitudes in (2.7) satisfy the *complex* linear system of ordinary differential equations

$$\mathcal{L}_{11}(W) + \mathcal{L}_{12}(F) = 0\,, \qquad \mathcal{L}_{21}(W) + \mathcal{L}_{22}(F) = 0\,, \tag{2.8}$$

where

$$\mathcal{L}_{ij} \equiv \begin{cases} \displaystyle\sum_{k=0}^{4}\mathcal{A}_{ijk}\frac{d^k}{d\phi^k}\,, & \text{if } (i,j) = (1,1) \text{ or } (i,j) = (2,2)\,, \\ \displaystyle\sum_{k=0}^{2}\mathcal{A}_{ijk}\frac{d^k}{d\phi^k}\,, & \text{if } (i,j) = (1,2) \text{ or } (i,j) = (2,1)\,, \end{cases}$$

and the definitions of the coefficients $\mathcal{A}_{ijk}$ are listed in Appendix A.

The equations (2.8) are to be solved subject to the following boundary conditions consistent with the scenario mentioned at the beginning of this section,

$$W = \frac{dW}{d\phi} = 0\,, \qquad \text{for } \phi = 0, \phi_0\,, \tag{2.9a}$$

$$F = \frac{dF}{d\phi} = 0\,, \qquad \text{for } \phi = 0, \phi_0\,. \tag{2.9b}$$

This completes the description of the key equations used in the rest of the paper. The linear differential system (2.8) together with the boundary conditions recorded above define a boundary eigenvalue problem in which $\lambda \equiv \lambda(m;\mu)$ plays the role of eigenvalue. It is further noted that $m \in \mathbb{N}$ is also unknown at this stage and, for each fixed ϕ_0, this parameter will have to be determined such that it renders the global minimum of the curve λ versus m (which would roughly correspond to a minimum-energy configuration reached by the deformed shell, e.g., see [9, 30]). As it is customary in problems of this type, the mode number will be regarded as a positive continuous parameter, i.e., $m \in \mathbb{R}_+$; the *critical eigenvalue*, λ_c, and the *critical mode number*, m_c, are thus defined by the requirements

$$\lambda_c = \min_{m>0} \lambda(m;\mu)\,, \qquad \text{with} \quad \lambda_c = \lambda(m_c;\mu)\,. \tag{2.10}$$

In order to gain insight into the structure that underpins our bifurcation system (2.8)-(2.9), we now turn to some direct numerical simulations of those equations. All numerical results reported in the next section are obtained by using standard routines available in MATLAB.

3 Numerical results

The geometry of the truncated hemisphere is entirely defined by the terminal latitude angle ϕ_0 (see Figure 2). For consistency with the shallow-shell theory adopted in the previous section, we present a summary of some direct numerical simulations obtained for two choices of this angle: $\phi_0 = 23°30'$ (which corresponds to $\phi_0 \simeq 0.4$ rad) and $\phi_0 = 34°$ ($\simeq 0.6$ rad). The Poisson's ratio turns out to play a relatively passive secondary role in the questions of interest here, so we take $\nu = 0.3$ in all of our numerical experiments.

The dependence of the applied load (λ) on the mode number (m) is illustrated in Figure 3 for a sequence of increasing values of (R/h) – see the caption for full details. Only the partial curves associated with $m \leq m_c$ are shown since DMV-type bifurcation equations based on a linear membrane basic state always lead to λ vs. m curves that have a unique global minimum. In both windows the circular markers correspond to the critical values (m_c, λ_c) mentioned in (2.10); the locus of these global minima as $\mu \propto (R/h) \gg 1$ increases is indicated by the dashed (red) curve. It is clear from the results that both λ_c and m_c increase with μ, while simple numerical checks confirm that $\lambda_c = \mathcal{O}(\mu)$ and $m_c = \mathcal{O}(\mu^{1/2})$, an observation that will be fully exploited in the next section.

The tendency of the eigenmodes to localise near the upper rim of the truncated hemisphere as $\mu \gg 1$ increases is apparent in the samples of critical eigenmodes recorded in Figures 4 and 5. In the interest of brevity we include only the real and imaginary parts, $W_{\rm R}(\phi)$ and $W_{\rm I}(\phi)$, respectively, of the complex amplitude $W(\phi)$ defined in (2.7). A quick glance at the eigenmodes shown with a continuous line in both figures mentioned reveals that they all consist of a relatively fast spatial oscillation modulated on a slower scale by a localised envelope. This second structure appears to be compressed in a narrow region adjacent to the upper rim of the hemisphere; it will be confirmed shortly that this

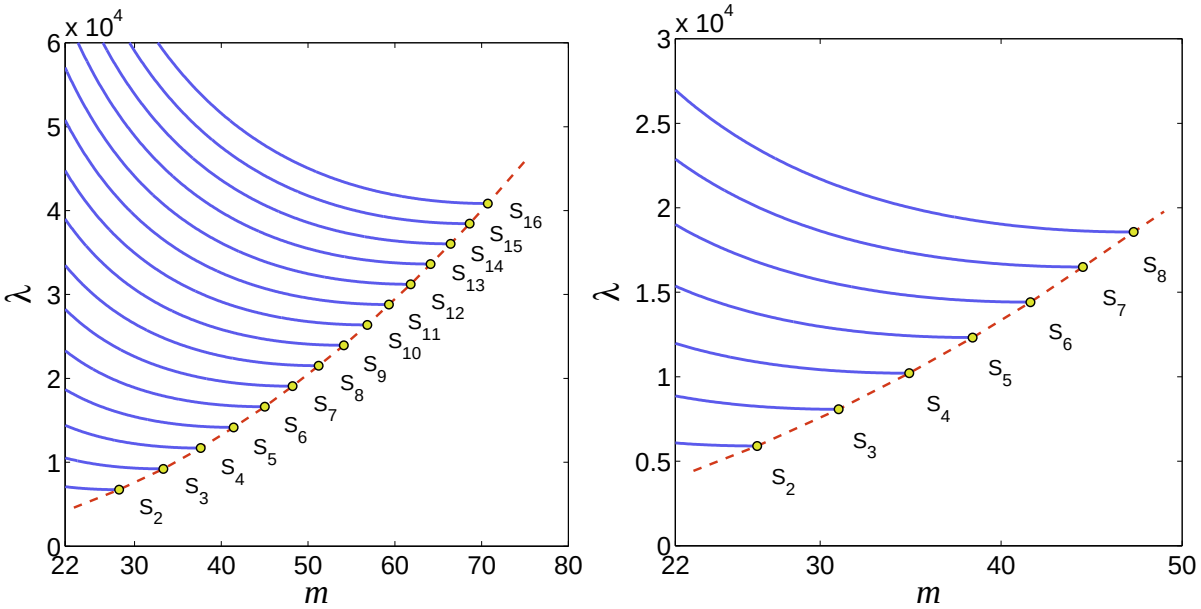

Figure 3: Dependence of the non-dimensional load λ on the mode number m for two geometries of the truncated hemisphere: $\phi_0 = 23^\circ\,30'$ (*left*) and $\phi_0 = 34^\circ$ (*right*). In each window the points $S_j \equiv (m_c, \lambda_c)$ denote the minima of the respective curves and identify the corresponding critical values; $(R/h) = (2j+1) \times 10^2$ for $j = 2, 3, \ldots, 16$ on the left, and $j = 2, 3, \ldots, 8$ in the other window. Only those parts of the response curves with $m \leq m_c$ are shown; the Poisson's ratio is $\nu = 0.3$.

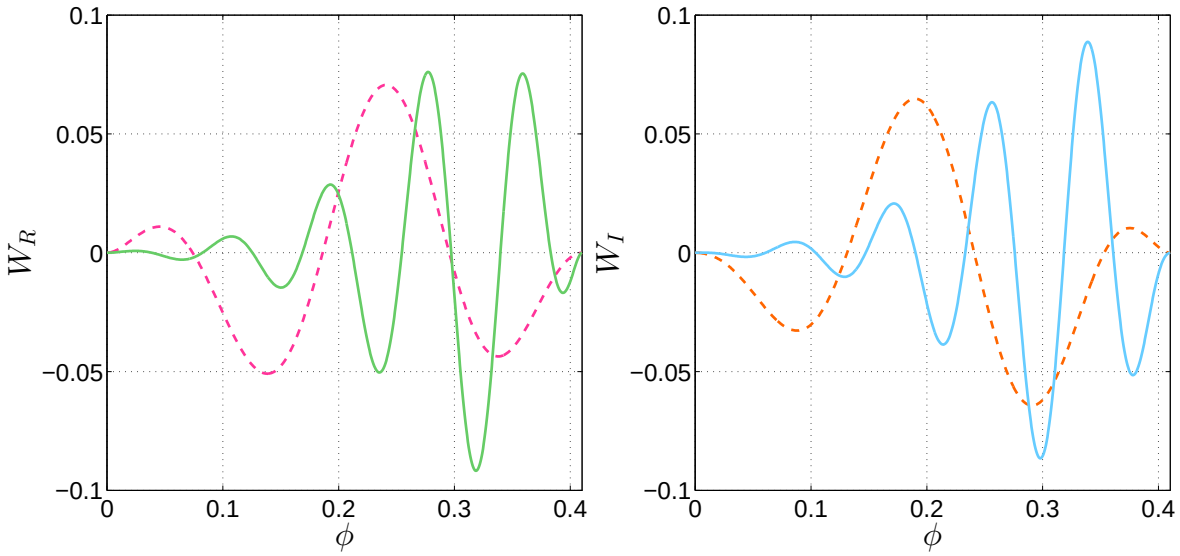

Figure 4: Two *critical eigenmodes* associated with the left window in Fig. 3 ($\phi_0 = 23^\circ\,30'$). These functions correspond to $R/h = 500$ (dashed line) and $R/h = 3300$ (continuous line), and illustrate the tendency to localisation of the lowest buckling mode as (R/h) increases. Both sets of solutions are normalised so that $\int_0^{\phi_0} \left[W_1^2(\phi) + W_2^2(\phi)\right] \mathrm{d}\phi = 0.001$.

envelope is actually the result of a (large) boundary-layer effect in the original eigenproblem, not much unlike the one found in the tensile loading scenario discussed by one of us in [12]. It is clear that the

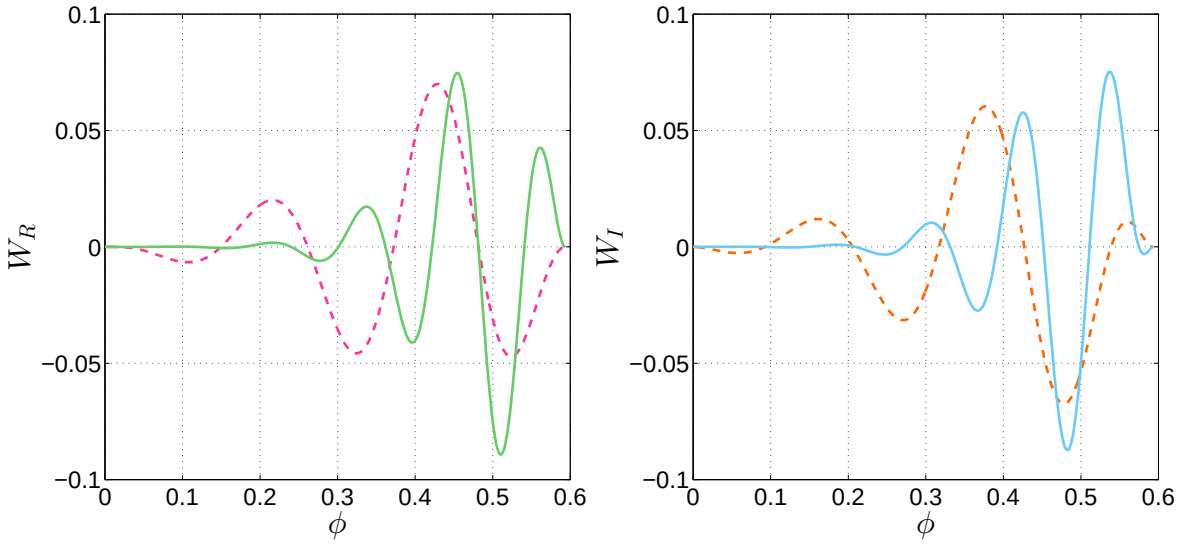

Figure 5: Same as in Fig. 4, except that here $\phi_0 = 34°$. The dashed-line eigenmodes correspond to $(R/h) = 500$, while the ones shown with the continuous line for $(R/h) = 1700$.

aforementioned localisation is not immediately forthcoming for the smaller value of ϕ_0 considered here – see Figure 4 (in particular, this also accounts for the larger values of (R/h) used in the left window of Figure 3). However, this is to be expected since in that case the size of μ is offset by the small latitudinal span $0 \leq \phi \leq \phi_0$ over which the differential equations (2.8) are integrated. Nevertheless, the localisation phenomenon is more prominent in Figure 5, which corresponds to $\phi_0 = 34°$. These observations suggest that in the large-μ limit, the solutions of the rather complicated boundary-value problem (2.8)-(2.9) ought to be amenable to asymptotic simplification. While, in principle, such simplifications would only be valid for $\mu \gg 1$, past experience shows that asymptotic formulae often prove to be useful to approximate even at moderate or low values of the perturbation parameter (e.g., see [12, 20, 25, 64]).

4 The main asymptotic structure

In the previous section we have seen that when the geometrical parameter $\mu \gg 1$, the critical modes of the torsion eigensystem adopt a structure that, broadly speaking, consists of two length-scales: a main region attached to the smaller rim ($\phi = \phi_0$), together with a spatial oscillation. Since the edges of spherical shell are restrained against transverse rotations, we can also anticipate from the outset the presence of a third length-scale associated with the ubiquitous *bending layer* found in many similar related scenarios (e.g., [16, 17, 19]).

We can examine the structure of the linearised equations (2.8) to motivate a number of the key scalings. If we balance the largest terms in $\mathcal{A}_{110}$ and $\mathcal{A}_{120}$ and between $\mathcal{A}_{210}$ and $\mathcal{A}_{220}$ then we would require that $m^4 W \sim \mu^2 m^2 F$ and $m^4 F \sim m^2 W$ pointing us to the fact that $m \sim \mu^{1/2}$. Moreover, in order to invoke spatial dependence in the solution we would anticipate that close to the rim we have $\phi = \phi_0 + \Delta$ and that $\mathcal{A}_{112}(d^2/d\phi^2) \sim \mathcal{A}_{110}\Delta$ which leads to the expectation that $\Delta \sim \mu^{-1/3}$. These arguments are entirely analogous to those reported in an earlier study (see [12]) and it can be confirmed *a priori* that the eigenmodes of our problem indeed reside within a relatively large boundary layer of thickness $\Delta = \mathcal{O}(\mu^{-1/3})$. This suggests the introduction of the re-scaled independent variable

Y defined by

$$\phi = \phi_0 - \mu^{-1/3} Y \qquad \text{with} \qquad Y = \mathcal{O}(1)\,. \tag{4.1}$$

By letting

$$\boldsymbol{u} := \begin{bmatrix} W \\ \mu F \end{bmatrix}, \qquad \boldsymbol{v}^{(j)}(Y) := \begin{bmatrix} W_j(Y) \\ F_j(Y) \end{bmatrix}, \qquad (j = 0, 1, 2, \dots)\,,$$

we look for solutions of (2.8) satisfying an ansatz of the form

$$\boldsymbol{u} = \boldsymbol{v}(Y) \exp(\mathrm{i}\kappa\mu^{1/6} Y)\,, \tag{4.2}$$

where

$$m = M_0 \mu^{1/2} + M_1 \mu^{1/6} + \dots\,, \tag{4.3a}$$

$$\lambda = \lambda_0 \mu + \lambda_1 \mu^{2/3} + \lambda_2 \mu^{1/2} + \lambda_3 \mu^{1/3} + \dots\,, \tag{4.3b}$$

$$\boldsymbol{v}(Y) = \boldsymbol{v}^{(0)}(Y) + \mu^{-1/6} \boldsymbol{v}^{(1)}(Y) + \mu^{-1/3} \boldsymbol{v}^{(2)}(Y) + \mu^{-1/2} \boldsymbol{v}^{(3)}(Y) + \mu^{-2/3} \boldsymbol{v}^{(4)}(Y) + \dots\,; \tag{4.3c}$$

the constant $\kappa \in \mathbb{R}$ is unknown at this stage but will be found as part of the solution. The complex exponential term in (4.2) accounts for the spatial oscillations of the eigenmodes seen in §3 – these oscillations take place on a $\mathcal{O}(\mu^{-1/2})$ scale (which is much shorter than that described by the rescaled independent variable Y in (4.1)). In principle, one can use the method of multiple scales (e.g., see [8, 49]) to achieve comparable results to the ansatz (4.2); however, guided by our past experience with similar situations (e.g., [14, 15]), we prefer to follow the more expedient route suggested by the above asymptotic expansions.

The constants M_j, $\lambda_j = \mathcal{O}(1)$ in (4.3a,4.3b), as well as the individual terms $\boldsymbol{v}^{(j)}(Y)$ on the right-hand side of (4.3c), are found as usual by substituting the assumed form of the solution in the original differential equations, collecting like powers of μ, and then setting to zero the corresponding coefficients. The outcome is a hierarchy of coupled algebraic equations that can be cast in the form

$$\boldsymbol{A}\boldsymbol{u}^{(j)} = \boldsymbol{b}^{(j)}\,, \qquad (j = 0, 1, 2, \dots)\,, \tag{4.4}$$

with

$$\boldsymbol{A} := \begin{bmatrix} \lambda_0 \kappa M_0 \sec^3\phi_0 + (\kappa^2 + M_0^2 \sec^2\phi_0)^2 & \kappa^2 + M_0^2 \sec^2\phi_0 \\ -(\kappa^2 + M_0^2 \sec^2\phi_0) & (\kappa^2 + M_0^2 \sec^2\phi_0)^2 \end{bmatrix}, \qquad \boldsymbol{b}^{(j)} := \begin{bmatrix} \mathcal{R}_{j1}, \\ \mathcal{R}_{j2} \end{bmatrix};$$

the expressions of the individual components of $\boldsymbol{b}^{(j)}$ are rather complicated and will be recorded separately as we go along.

The zeroth-order equations correspond to $\mathcal{R}_{01} = \mathcal{R}_{02} \equiv 0$, so we are left with a *homogeneous* linear system. The existence of non-trivial solutions requires that $\det(\boldsymbol{A}) = 0$, whence

$$\lambda_0 \kappa M_0 \sec^3\phi_0 + (\kappa^2 + M_0^2 \sec^2\phi_0)^2 + 1 = 0\,. \tag{4.5}$$

We note in passing that this relation suggests that $\kappa < 0$; it is also clear from (4.5) that $\lambda_0 \equiv \lambda_0(M_0, \kappa)$, with

$$\lambda_0(M_0, \kappa) := -\frac{(\kappa^2 + M_0^2 \sec^2\phi_0)^2 + 1}{\kappa M_0 \sec^3\phi_0}\,. \tag{4.6}$$

In light of our earlier comments vis-à-vis (2.10), we must search for the critical values of λ_0 and M_0 by enforcing the criticality conditions

$$\frac{\partial \lambda_0}{\partial M_0} = \frac{\partial \lambda_0}{\partial \kappa} = 0$$

for the function defined in (4.6). In conjunction with (4.5), these two simultaneous equations yield

$$\lambda_0 = 4\cos^2\phi_0\,, \qquad M_0 = \frac{\cos\phi_0}{\sqrt{2}}\,, \qquad \kappa = -\frac{1}{\sqrt{2}}\,. \tag{4.7}$$

An immediate consequence of the particular numerical values recorded in (4.7) is that

$$W_0 \equiv F_0\,, \tag{4.8}$$

which is largely responsible for the simplification of most of the subsequent algebraic manipulations.

The solvability condition for the remaining inhomogeneous systems (4.4) with $j \geq 1$ requires that the solution of the corresponding adjoint is orthogonal to the vectors $\boldsymbol{b}^{(j)}$; this adjoint solution is simply $[-1,\ 1]$, so the aforementioned solvability requirement becomes $\mathcal{R}_{j1} - \mathcal{R}_{j2} = 0$ for $j \geq 1$.

The components of the right-hand side of (4.4) for the first-order equations are found to be

$$\mathcal{R}_{11} := -\mathrm{i}\sqrt{2}F_0'\,, \qquad \mathcal{R}_{12} := -2\mathrm{i}\sqrt{2}\kappa F_0' + \mathrm{i}\sqrt{2}W_0'\,, \tag{4.9}$$

where the 'dash' stands for differentiation with respect to Y. The solvability condition is automatically satisfied owing to (4.8), and we remark that

$$F_1 = W_1 - \mathrm{i}\sqrt{2}W_0'\,. \tag{4.10}$$

The leading-order eigenfunctions (W_0 and F_0) remain unknown at this stage, but will be determined at the next order.

Routine algebraic manipulations show that the right-hand sides of the equations at second-order have components

$$\mathcal{R}_{21} := 3W_0'' - 3Y\tan\phi_0 W_0 + \frac{1}{2}\lambda_1\sec^2\phi_0 W_0 - \mathrm{i}\sqrt{2}W_1' - M_1\sqrt{2}\sec\phi_0 W_0\,, \tag{4.11a}$$

$$\mathcal{R}_{22} := -W_0'' + Y\tan\phi_0 W_0 - \mathrm{i}\sqrt{2}W_1' - M_1\sqrt{2}\sec\phi_0 W_0\,. \tag{4.11b}$$

The consistency condition $\mathcal{R}_{21} - \mathcal{R}_{22} = 0$ leads immediately to a scaled Airy-type equation

$$W_0'' - (\Gamma_1 Y + \Gamma_2)W_0 = 0\,, \tag{4.12}$$

with

$$\Gamma_1 := \tan\phi_0 \qquad \text{and} \qquad \Gamma_2 := -\frac{1}{8}\lambda_1\sec^2\phi_0 \tag{4.13}$$

and we note also that

$$F_2 = W_2 - W_0'' + Y\tan\phi_0 W_0 - \mathrm{i}\sqrt{2}W_1' - M_1\sqrt{2}\sec\phi_0 W_0\,. \tag{4.14}$$

Equation (4.12) can be put into standard form by a suitable re-scaling of the independent variable

$$Z := \Gamma_1^{1/3} Y + \frac{\Gamma_2}{\Gamma_1^{2/3}}\,, \tag{4.15}$$

whereupon it follows that $d^2\widehat{W}_0/dZ^2 - Z\widehat{W}_0 = 0$, with $\widehat{W}_0(Z) \equiv W_0(Y)$. The solution of interest is $\widehat{W}_0 = (1+\mathrm{i})\mathrm{Ai}(Z)$, where 'Ai' is the usual Airy function that decays exponentially quickly as $Z \to +\infty$.

The boundary conditions (2.9) at $\phi = \phi_0$ (i.e., at $Y = 0$) cannot both be imposed – this suggests that the main $Y = \mathcal{O}(1)$ region must be supplemented by an inner zone, but we demand that $W_0 \to 0$ as $Y \to 0^+$. We recall in passing that, in addition to decaying exponentially as $Z \to +\infty$, the Airy function possesses a countable set of zeros along the negative Z-axis; the first occurs at $(-\zeta_0) \simeq -2.338$, so we can ensure that $W_0(Y) = 0$ at $Y = 0$ by demanding $\Gamma_1^{-2/3}\Gamma_2 = -\zeta_0$. If the expressions (4.13) are substituted in this relation, it follows immediately that

$$\lambda_1 = 8\zeta_0 \cos^2\phi_0 \tan^{2/3}\phi_0 \,. \tag{4.16}$$

The two-term approximation of λ available at this stage performs remarkably well, but it represents an upper bound for the value determined by numerically solving the original torsion eigenproblem; this is illustrated in Figure 6 for which $\phi_0 = 23°30'$. The dependence of the one-term approximation $\lambda_c \simeq \lambda_0\mu$ as a function of (R/h) corresponds to the dashed (green) curve. Superimposed on the same plot are the two-term approximation $\lambda_c \simeq \lambda_0\mu + \lambda_1\mu^{2/3}$ (red curve) together with the corresponding results obtained from direct numerical simulations of (2.8)-(2.9); this latter set of values is shown as the discrete (blue) markers joined by a dashed (blue) line. On the scale of the plot shown in Figure 6 the two-term approximation is almost indistinguishable from the "true" values of λ_c (obtained by direct numerical simulations of the original eigenproblem), but the inset provides further details regarding the relative position of the various sets of data used in that plot. A further sample of similar comparisons is included in Figure 7 now with $\phi_0 = 34°$. The relative errors of the two-term approximation seen in the right window of that figure are representative for all angles $23°30' \le \phi_0 \le 34°$.

At this stage it seems sensible to enquire as to the "fate" of the two-term approximation derived above; in particular, it would be desirable to know whether the addition of the next few terms in the ansatz (4.3b) will improve the present accuracy. This would normally be expected since the analysis carried out so far has not taken into account the presence of the bending boundary layer associated with the flexurally clamped boundary constraints (2.9). However, the result turns out to be rather unexpected, and we are going to show eventually that the addition of further terms in the expansion of λ_c can actually lead to a slight deterioration in the accuracy of the approximation.

With this in mind, our immediate goal is to calculate the λ_2-term in the expansion (4.3b); as the algebraic expressions involved are more complicated than in the previous cases, we will confine ourselves to giving only an outline of the main calculations.

Imposing the solvability condition $\mathcal{R}_{31} - \mathcal{R}_{32} = 0$ on the third-order system we find an inhomogeneous version of the differential equation (4.12) in which $W_0(Y)$ is replaced by $W_1(Y)$. With the aid of the change of variable (4.15) this equation is transformed to

$$\frac{d^2\widehat{W}_1}{dZ^2} - Z\widehat{W}_1 = B_1\widehat{W}_0(Z) + B_2 Z\widehat{W}_0^{(1)} \,, \tag{4.17}$$

where

$$B_1 \equiv -\frac{1}{8}\lambda_2 \sec^2\phi_0 \tan^{-2/3}\phi_0 \,, \qquad B_2 \equiv \frac{\mathrm{i}}{\sqrt{2}} \tan^{1/3}\phi_0 \,,$$

and the superscript on $\widehat{W}_0$ indicates differentiation with respect to Z. A particular solution of (4.17) is readily identified as

$$\widehat{W}_1(Z) = \frac{1}{4}B_2\widehat{W}_0^{(4)}(Z) + (B_1 - B_2)\widehat{W}_0^{(1)}(Z) \,. \tag{4.18}$$

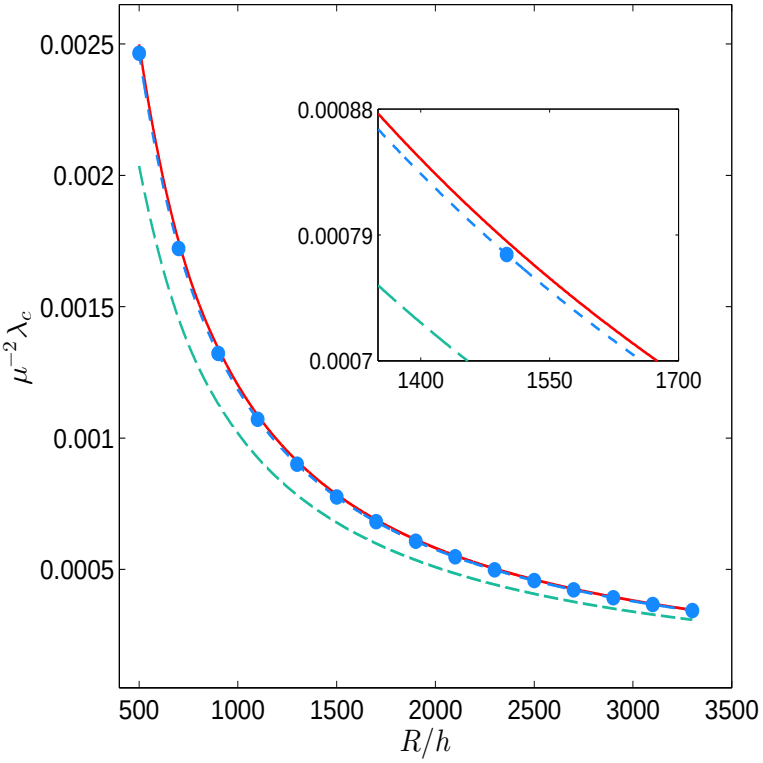

Figure 6: Comparison of the one- and two-term approximations (4.3b) with direct numerical simulations of the bifurcation equations (2.8) subject to the boundary conditions (2.9). The numerical results are shown with (blue) markers joined by a dashed curve; the one-term approximation corresponds to the (green) dashed curve, while the two-term approximation is indicated by the continuous (red) curve. The inset clarifies the relative positions of these three sets of data. Here $\phi_0 = 23°30'$.

It will prove necessary to evaluate both $\widehat{W}_1$ and its derivative at $Z = -\zeta_0$; simplified forms of these can be deduced by remembering that $d^2\widehat{W}_0/dZ^2 - Z\widehat{W}_0 = 0$ and that $\widehat{W}_0(-\zeta_0) = 0$. Repeated differentiation of this defining equation shows that $\widehat{W}_0^{(4)}(-\zeta_0) = 2\widehat{W}_0^{(1)}(-\zeta_0)$ and $\widehat{W}_0^{(5)}(-\zeta_0) = \zeta_0^2\widehat{W}_0^{(1)}(-\zeta_0)$ whence

$$\widehat{W}_1\big|_{Z=-\zeta_0} = \left(B_1 - \frac{1}{2}B_2\right)\widehat{W}_0^{(1)}(-\zeta_0) \quad \text{and} \quad \frac{d\widehat{W}_1}{dZ}\Big|_{Z=-\zeta_0} = \frac{1}{4}\zeta_0^2 B_2\widehat{W}_0^{(1)}(-\zeta_0)\,. \tag{4.19}$$

Given the complex-valued coefficients of equation (4.17) and the fact that $\widehat{W}_0$ itself is a complex function of $Z \in \mathbb{R}$, some care must be taken in interpreting these relations. To this end, we start off by writing

$$\widehat{W}_0 = \widehat{W}_{0\mathrm{R}} + \mathrm{i}\widehat{W}_{0\mathrm{I}} \qquad \text{and} \qquad \widehat{W}_1 = \widehat{W}_{1\mathrm{R}} + \mathrm{i}\widehat{W}_{1\mathrm{I}}\,,$$

where $\widehat{W}_{0\mathrm{R}} \equiv \widehat{W}_{0\mathrm{I}}$ and are both equal to the Airy function $\mathrm{Ai}(Z)$. The subscripts 'R' and 'I' refer to the real and imaginary parts, respectively, of the expressions in question – a convention that we will continue to employ henceforth. Separating the real and imaginary parts, the equations (4.19) can be cast in the more detailed form

$$\widehat{W}_{1\mathrm{R}}(-\zeta_0) = \left(B_1 - \frac{\mathrm{i}}{2}B_2\right)\mathrm{Ai}_0'\,, \qquad \widehat{W}_{1\mathrm{I}}(-\zeta_0) = \left(B_1 + \frac{\mathrm{i}}{2}B_2\right)\mathrm{Ai}_0'\,, \tag{4.20a}$$

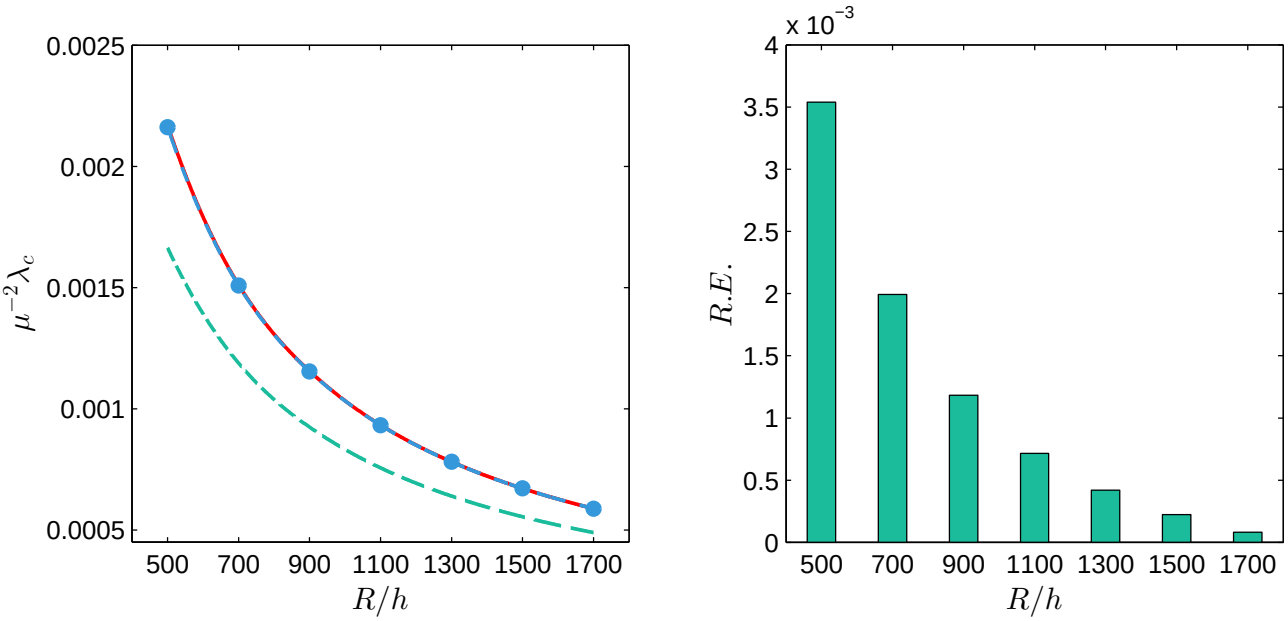

Figure 7: *Left:* same as in Fig. 6, but for $\phi_0 = 34°$. *Right:* the corresponding relative errors (*R.E.*) for the truncation of (4.3b) up to the $\mathcal{O}(\mu^{1/2})$ term (this truncation is referred to as the 'two-term approximation' of λ_c in the main text).

$$\left.\frac{d\widehat{W}_{1\mathrm{R}}}{dZ}\right|_{Z=-\zeta_0} = \frac{\mathrm{i}}{4}\zeta_0^2 B_2 \mathrm{Ai}_0' \,, \qquad \left.\frac{d\widehat{W}_{1\mathrm{I}}}{dZ}\right|_{Z=-\zeta_0} = -\frac{\mathrm{i}}{4}\zeta_0^2 B_2 \mathrm{Ai}_0' \,, \tag{4.20b}$$

where $\mathrm{Ai}_0' \equiv \mathrm{Ai}'(-\zeta_0)$.

5 The nested layer

It was noted in the previous section that, while we could make W_0 vanish on $Y = 0$, we could not satisfy the derivative condition part of (2.9a). This condition can be enforced by the introduction of a suitably thin *bending layer* whose extent is set by the expectation that this layer is comparable in size with the wavelength of the modes in the latitudinal co-ordinate θ. As we have predicated that the modes of interest have a wavenumber $m = \mathcal{O}(\mu^{1/2})$ this points us to a bending layer of depth $\mathcal{O}(\mu^{-1/2})$. We therefore introduce a new re-scaled coordinate X such that

$$\phi = \phi_0 - \mu^{-1/2} X \,, \qquad X = \mathcal{O}(1) \,. \tag{5.1}$$

By expressing the solutions of (2.8) in terms of X we will derive a new set of expansions that will have to be matched asymptotically to the expressions derived in the previous section. Given the presence of the fast spatial oscillation term '$\exp(\mathrm{i}\kappa\mu^{1/6}Y)$' in those results – see (4.2), we expect a similar structure for the solutions in the bending layer (otherwise the matching of the two sets of functions fails). Note that expressed in terms of the new rescaled variable in (5.1) this exponential becomes '$\exp(\mathrm{i}\kappa X)$'.

After these preliminary observations we are now ready to introduce the rest of the details for the analysis of our secondary boundary layer. In particular, the transverse displacement and the stress function amplitudes in (2.8) will be sought in the forms

$$W = g(X)\exp(\mathrm{i}\kappa X) \,, \qquad F = f(X)\exp(\mathrm{i}\kappa X) \,, \tag{5.2}$$

with

$$g = \mu^{-1/6} g_0(X) + \mu^{-1/3} g_1(X) + \dots \qquad \text{and} \qquad f = \mu^{-7/6} f_0(X) + \mu^{-4/3} f_1(X) + \dots \,, \tag{5.3}$$

where g_j, f_j $(j \geq 0)$ will be determined sequentially as explained next. To this end we note that the boundary conditions at the upper rim of our shell – see (2.9), will assume the form

$$g_0 = f_0 = \frac{dg_0}{dX} = \frac{df_0}{dX} = 0\,, \qquad \text{for} \quad X = 0\,, \tag{5.4}$$

and the coefficients of our boundary-layer ansatz will also be subject to the usual conditions that f_0 and g_0 do not grow exponentially as $X \to +\infty$.

Standard calculations reveal that the leading-order approximation corresponding to (5.3) satisfies the differential system

$$\begin{bmatrix} (D^2 - \mathrm{i}\sqrt{2}D - 1)^2 - 2(\mathrm{i}\sqrt{2}D + 1) & -(D^2 - \mathrm{i}\sqrt{2}D - 1) \\ D^2 - \mathrm{i}\sqrt{2}D - 1 & (D^2 - \mathrm{i}\sqrt{2}D - 1)^2 \end{bmatrix} \begin{bmatrix} g_0(X) \\ f_0(X) \end{bmatrix} = \begin{bmatrix} 0 \\ 0 \end{bmatrix}, \tag{5.5}$$

with $D \equiv d/dX$. Since this is a constant-coefficient problem we look for solutions in the form $g_0 = \widehat{g}_0 \exp(pX)$ and $f_0 = \widehat{f}_0 \exp(pX)$, where the complex numbers p, $\widehat{g}_0$ and $\widehat{f}_0$ are readily found as explained next.

The characteristic equation satisfied by p turns out to be

$$p^2(p^2 - \mathrm{i}\sqrt{2}p - 1)^2(p^2 - 2\mathrm{i}\sqrt{2}p - 4) = 0\,,$$

which has the non-trivial roots

$$p_1 = p_2 := \frac{1+\mathrm{i}}{\sqrt{2}}\,, \qquad p_3 = p_4 := \frac{-1+\mathrm{i}}{\sqrt{2}}\,, \qquad p_5 := \sqrt{2}(1+\mathrm{i})\,, \qquad p_6 := \sqrt{2}(-1+\mathrm{i})\,, \tag{5.6}$$

in addition to the double-root $p_7 = p_8 := 0$. Thus, the solutions of (5.5) will be linear combinations of complex exponentials. The details of the solution procedure are relegated to Appendix B; here we only state the final results

$$g_0(X) = \gamma_0\big[-2\mathrm{e}^{p_4 X} + (2+\mathrm{i})\mathrm{e}^{p_6 X} + (2\sqrt{2}X - \mathrm{i})\big]\,, \tag{5.7a}$$

$$f_0(X) = \gamma_0\big[-\mathrm{i}\mathrm{e}^{p_6 X} + 2\mathrm{i}(3 + X\sqrt{2})\mathrm{e}^{p_4 X} + (2\sqrt{2}X - 5\mathrm{i})\big]\,, \tag{5.7b}$$

where $\gamma_0 \in \mathbb{C}$ is arbitrary at this stage. We also mention that the functions $g_1(X)$ and $f_1(X)$ in the expansions (5.3) turn out to be precisely of the same form as (5.7) save that γ_0 must be replaced by a new multiplicative constant $\gamma_1 \in \mathbb{C}$.

6 Matching the solutions at leading order

To fix λ_2 we must ensure that the solution in the main layer matches with the expressions (5.7) of the previous section. By writing

$$\gamma_0 = \gamma_{0\mathrm{R}} + \mathrm{i}\gamma_{0\mathrm{I}} \qquad \text{and} \qquad \gamma_1 = \gamma_{1\mathrm{R}} + \mathrm{i}\gamma_{1\mathrm{I}}$$

we note that the relevant terms from the nested layer that are relevant to the matching comprise of the following at $\mathcal{O}(\mu^{-1/6})$ and $\mathcal{O}(\mu^{-1/3})$ so that

$$\gamma_j(2\sqrt{2}X - \mathrm{i}) = \big(2\sqrt{2}\gamma_{j\mathrm{R}}X + \gamma_{j\mathrm{I}}\big) + \mathrm{i}\big(2\sqrt{2}\gamma_{j\mathrm{I}}X - \gamma_{j\mathrm{R}}\big)\,, \tag{6.1}$$

where $j = 0$ and $j = 1$, respectively. These expressions have to be blended to the relevant parts of the solution in the main layer. Given that $\Re\{\widehat{W}_0\}, \Im\{\widehat{W}_0\} \propto \mathrm{Ai}(Z)$, and we recall the definition (4.15) for Z, it transpires that when $Y = \mu^{-1/6}X$ we have

$$\widehat{W}_0 = \mu^{-1/6}\Gamma_1\beta_{01}X + \mathcal{O}(\mu^{-1/2})$$

and, similarly, we find that

$$\widehat{W}_1 = \beta_{10} + \mu^{-1/6}\Gamma_1\beta_{11}X + \mathcal{O}(\mu^{-1/3})$$

where the constants $\beta_{ij} \in \mathbb{C}$ are defined by

$$\beta_{ij} := \begin{cases} \dfrac{d^j\widehat{W}_i}{dZ^j}\Big|_{Z=-\zeta_0} & \text{if} \quad j \geq 1\,, \\[2ex] \widehat{W}_i(-\zeta_0) & \text{if} \quad j = 0\,. \end{cases}$$

According to these elementary observations, the solution in the main layer expands according to

$$W = \mu^{-1/6}\underline{(\Gamma_1\beta_{01}X + \beta_{10})} + \mu^{-1/3}(\Gamma_1^{1/3}\beta_{11}X + \beta_{20}) + \dots\,, \tag{6.2}$$

and at this stage we can only match the underlined expressions in (6.2) with those on the right-hand side of the equality sign in (6.1) corresponding to $j = 1$. In terms of the real and imaginary parts of $\widehat{W}_1$, this requirement translates into the following conditions

$$(\tan^{1/3}\phi_0)\mathrm{Ai}_0' = 2\sqrt{2}\gamma_{0\mathrm{R}}\,, \qquad (\tan^{1/3}\phi_0)\mathrm{Ai}_0' = 2\sqrt{2}\gamma_{0\mathrm{I}}\,, \tag{6.3a}$$

$$\widehat{W}_{1R}\big|_{Z=-\zeta_0} = \gamma_{0\mathrm{I}}\,, \qquad \widehat{W}_{1I}\big|_{Z=-\zeta_0} = -\gamma_{0\mathrm{R}}\,, \tag{6.3b}$$

whence

$$\gamma_{0\mathrm{R}} = \gamma_{0\mathrm{I}} = \left(\frac{\mathrm{Ai}_0'}{2\sqrt{2}}\right)\tan^{1/3}\phi_0\,.$$

Using the expressions (4.20a) found earlier in §4, we also deduce from (6.3b) that $B_1 = 0$ and hence

$$\lambda_2 = 0\,. \tag{6.4}$$

Since the $\mathcal{O}(\mu^{1/2})$-correction term for the critical load happens to vanish, we have to move onto the next-order term λ_3 in order to ascertain whether the correction to the simple two-term result is positive or negative. As it will become clear shortly, the coefficient M_1 in the expansion (4.3a) will also be determined at the same time as λ_3. The relevant calculations are outlined below.

7 The λ_3 term and higher-order matching

The coefficient λ_3 in (4.3b) will be tied down by enforcing higher-order matching conditions between the main asymptotic structure of §4 and the bending layer discussed in §5. To this end, we now turn our attention to the solvability condition $\mathcal{R}_{41} - \mathcal{R}_{42} = 0$ for the fourth-order system. The result can be shown to be an inhomogeneous differential equation in $W_2 \equiv W_2(Y)$. In order to take advantage of the Airy equation found in our earlier second-order calculations, we use (4.15) to express the results in terms of Z,

$$\frac{d^2\widehat{W}_2}{dZ^2} - Z\widehat{W}_2 = (C_1 + C_2Z + C_3Z^2)\widehat{W}_0(Z) + (C_4 + C_5Z^3)\widehat{W}_0^{(1)}(Z) \tag{7.1}$$

with

$$C_1 := -M_1\zeta_0\sqrt{2}\sec\phi_0 - \left(\frac{1}{8}\lambda_3 - M_1^2\right)\sec^2\phi_0\tan^{-2/3}\phi_0 - \left(\frac{1}{2}\tan^{-4/3}\phi_0 - \tan^{2/3}\phi_0\right)\zeta_0^2\,, \quad (7.2a)$$

$$C_2 := -\frac{M_1}{\sqrt{2}}\sec\phi_0 - \zeta_0\tan^{-4/3}\phi_0 - \frac{1}{2}\zeta_0\tan^{2/3}\phi_0\,, \qquad C_3 := -\frac{1}{2}\tan^{-4/3}\phi_0 - \frac{3}{4}\tan^{2/3}\phi_0\,, \quad (7.2b)$$

$$C_4 := \frac{1}{2}\tan^{2/3}\phi_0\,, \qquad C_5 := -\frac{1}{8}\tan^{2/3}\phi_0\,. \quad (7.2c)$$

It is easily checked that a particular solution of (7.1) is given by

$$\widehat{W}_2(Z) = C_1\widehat{W}_0^{(1)}(Z) + \left(-C_3 + \frac{1}{2}C_4 + 4C_5\right)\widehat{W}_0^{(2)}(Z) + \frac{1}{3}C_2\widehat{W}_0^{(3)}(Z) + \frac{1}{5}(C_3 - 9C_5)\widehat{W}_0^{(5)}(Z) + \frac{1}{8}C_5\widehat{W}_0^{(8)}(Z)\,. \quad (7.3)$$

For matching with the solution in the nested layer, we need the value of this function as $Z \to (-\zeta_0)$, and it is a simple exercise to show that

$$\widehat{W}_2\Big|_{Z=-\zeta_0} = \left[C_1 - \frac{1}{3}C_2\zeta_0 + \frac{1}{10}\left(2C_3 - 3C_5\right)\xi_0^2\right]\widehat{W}_0^{(1)}(-\zeta_0)\,. \quad (7.4)$$

By using the definitions of the coefficients C_j recorded above, the expression in (7.4) can be re-arranged as a quadratic in M_1,

$$\widehat{W}_2\Big|_{Z=-\zeta_0} = (1+\mathrm{i})(q_2M_1^2 + q_1M_1 + q_0)\mathrm{Ai}_0'\,, \quad (7.5)$$

in which

$$q_0 := \left(\frac{253}{240}\tan^{2/3}\phi_0 - \frac{4}{15}\tan^{-4/3}\phi_0\right)\zeta_0^2 - \frac{1}{8}\lambda_3\sec^2\phi_0\tan^{-2/3}\phi_0\,,$$

$$q_1 := -\frac{5\zeta_0}{3\sqrt{2}}\sec\phi_0\,, \quad \text{and} \quad q_2 := \sec^2\phi_0\tan^{-2/3}\phi_0\,.$$

To complete the derivation of λ_3 and fix M_1, we need to return to the asymptotic matching of (6.1) and the remaining terms in (6.2). Comparing the relevant parts of those expressions we discover that

$$-\frac{\zeta_0^2}{4\sqrt{2}}(\tan^{2/3}\phi_0)\mathrm{Ai}_0' = 2\sqrt{2}\gamma_{1\mathrm{R}}\,, \qquad \frac{\zeta_0^2}{4\sqrt{2}}(\tan^{2/3}\phi_0)\mathrm{Ai}_0' = 2\sqrt{2}\gamma_{1\mathrm{I}}\,, \quad (7.6a)$$

$$\widehat{W}_{2R}\big|_{Z=-\zeta_0} = \gamma_{1\mathrm{I}}\,, \qquad \widehat{W}_{2I}\big|_{Z=-\zeta_0} = -\gamma_{1\mathrm{R}}\,, \quad (7.6b)$$

Since the coefficients C_j that appear in (7.2) are all real-valued, $\widehat{W}_2(Z)$ will have the same real and imaginary parts, and their common value is given by (7.3) in which $\widehat{W}_0(Z)$ is replaced by the Airy function $\mathrm{Ai}(Z)$. With this observation in mind, it should be clear that (7.6b) collapse to the single equation

$$\widehat{W}_2\Big|_{Z=-\zeta_0} = (1+\mathrm{i})\frac{\zeta_0^2}{16}\tan^{2/3}\phi_0\mathrm{Ai}_0'\,.$$

In conclusion, this result, when used in conjunction with (7.5), will provide us with a quadratic of the form $\lambda_3 \equiv \lambda_3(M_1)$. Minimizing its value with respect to M_1 yields

$$M_1 = \frac{5\zeta_0}{6\sqrt{2}} \cos\phi_0 \tan^{2/3}\phi_0 \,, \tag{7.7}$$

whereupon

$$\lambda_3 = \frac{4\zeta_0^2(17 - 41\cos 2\phi_0)}{45\tan^{2/3}\phi_0} \,. \tag{7.8}$$

Unlike the previously determined coefficients, λ_0 and λ_1, the value of λ_3 can be positive or negative; it switches sign when $\phi_0 \simeq \phi_0^* := 32.75°$. We also note that $\lambda_3(\phi_0) < 0$ for $\phi_0 < \phi_0^*$, and refer to Figure 8 for further quantitative information about the size of this coefficient; the variation of $\lambda_0(\phi_0)$ and $\lambda_1(\phi_0)$ is included for the sake of completeness. It is therefore clear that the addition of the λ_3-term in the formula (4.3b) has the potential of improving the accuracy of the two-term approximation discussed at the end of §4. However, for $\phi_0 > \phi_0^*$ this is no longer true and, in fact, one would expect the predictions of the three-term approximation to move farther away from the true value of λ_c.

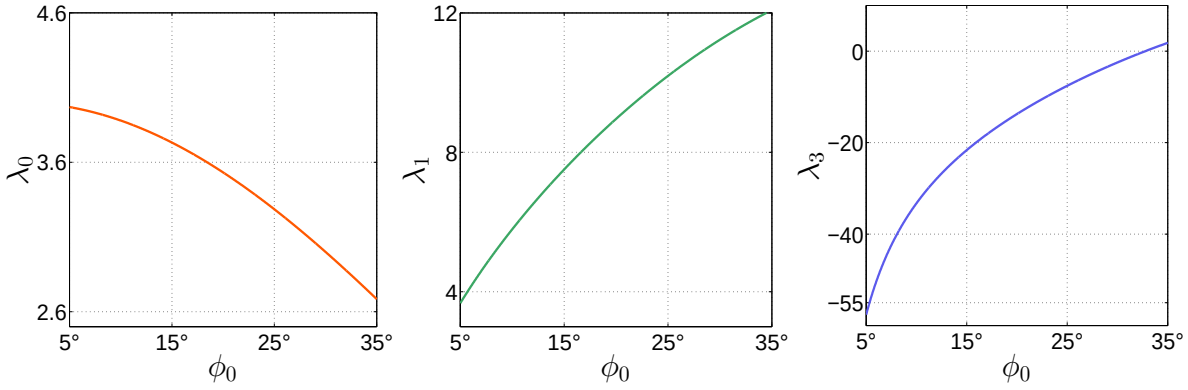

Figure 8: The variation of the non-zero coefficients $\lambda_j \equiv \lambda_j(\phi_0)$ $(j = 0, 1, 3)$ in the asymptotic expansion (4.3b) for the critical load λ_c.

The claims made in the previous paragraph are corroborated by the comparisons between the three-term formula $\lambda_c \simeq \lambda_0\mu + \lambda_1\mu^{2/3} + \lambda_3\mu^{1/3}$ and the direct numerical simulations of the original boundary-value problem. This information can be seen in Figure 9, where we have used the same two values of ϕ_0 as in §3: $23°30'$ (left) and $34°$ (right). While in both windows the three-term theoretical predictions are very close to the true values, the close-up detail shown in the inset confirms that for the smaller terminal latitude angle there is a decrease in relative accuracy, while in the other case we get exactly the opposite effect.

Our asymptotic predictions of (4.3a) for the critical number of wrinkles associated with the onset of instability are recorded in Figure 10, for the same two values of ϕ_0 as in the previous figure. The relative errors of these predictions range from 8% to 4% in the left window, and from 10% to 7% in the right window. This modest accuracy is to be expected on several grounds. For example, the terms neglected in (4.3a) are (theoretically) of size $\mathcal{O}(\mu^{-1/6})$; another source of inaccuracy in the approximation of m_c can be linked to the discrete nature of this quantity that here was regarded as a continuous variable. Nevertheless, the relative errors mentioned are entirely consistent with previous similar studies on related problems (e.g., [15, 16, 18, 19]).

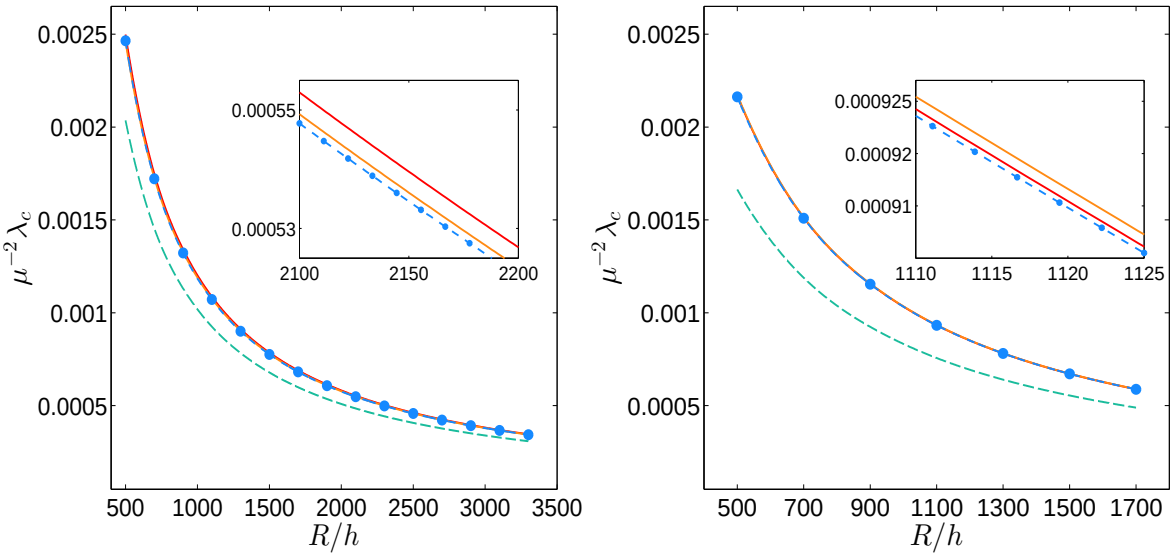

Figure 9: Comparisons of one-, two-, and three-term approximations (4.3b) with direct numerical simulations of the original boundary-value problem (2.8)-(2.9). On the left $\phi_0 = 23°30'$, while on the right $\phi_0 = 34°$. The three-term approximation is shown with a continuous (dark orange) curve, the two-term formula is given by the continuous (red) line, the one-term predictions correspond to the dashed (green) curve, and the direct numerical simulation are indicated by the (blue) circular markers joined by a dashed (blue) line. In the left window $\lambda_3(\phi_0) < 0$, while in the right one $\lambda_3(\phi_0) > 0$, a feature that has implications regarding the relative positions of the various data curves – see the details in each inset.

8 Concluding remarks

In this work we have provided a detailed asymptotic description of the eigendeformations associated with the torsional buckling for a truncated hemispherical, thin, elastic shell in which the upper rim experiences in-plane twisting relative to the other circular edge. One of our main interests has been in describing the tendency of these deformations to concentrate in a relatively narrow zone adjacent to the smaller rim of the shell, as the parameter $\mu \propto (R/h) \gg 1$ increases (with h and R being, respectively, the thickness and the radius of the shell). By using matched asymptotic expansions for a system of eight complex-valued ordinary differential equations we have derived a number of practical approximations for the critical torque (λ_c) in terms of suitable powers of the asymptotic parameter μ mentioned above – see formula (4.3b) in which the coefficients λ_j ($j = 0, 1, 2, 3$) have to be replaced by the values recorded in (4.7), (4.16), (6.4) and (7.8). For the sake of completeness, this result is also expressed in terms of the physical quantities and is recorded below,

$$\frac{M_c}{\pi R h^2 E} = \beta_1(1-\nu^2)^{-1/2}\cos^2\phi_0 + \beta_2(1-\nu^2)^{-2/3}\cos^2\phi_0\tan^{2/3}\phi_0\left(\frac{h}{R}\right)^{1/3}$$
$$+\,\beta_3(1-\nu^2)^{-5/6}\left(\frac{17-41\cos 2\phi_0}{\tan^{2/3}\phi_0}\right)\left(\frac{h}{R}\right)^{2/3} + \dots\,, \quad (8.1)$$

where

$$\beta_1 \simeq 1.1547\,, \qquad \beta_2 \simeq 3.5685\,, \qquad \beta_3 \simeq 0.0613\,.$$

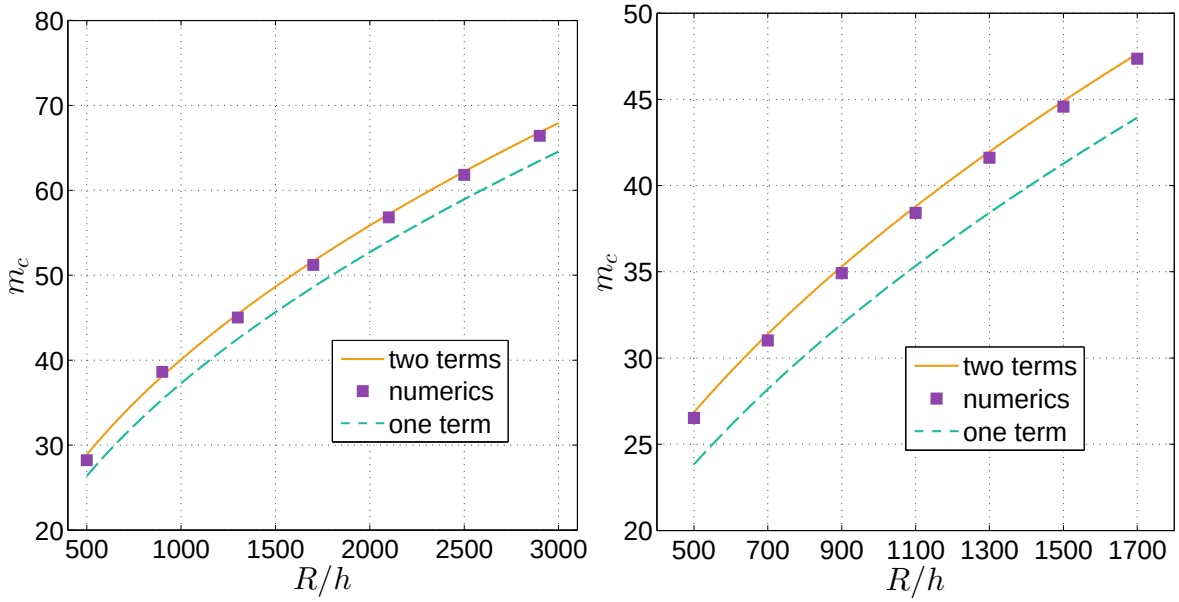

Figure 10: Comparison between the asymptotic approximations of the critical mode number (4.3a) and the direct numerical simulations of the original bifurcation problem (2.8)-(2.9): $\phi_0 = 23°30'$ (*left*) and $\phi_0 = 34°$ (*right*). In each window the square markers correspond to the numerical results; the dashed line represents the one-term approximation obtained from (4.3a) by neglecting the $\mathcal{O}(\mu^{1/6})$ term; the continuous line is used for the full form of (4.3a) which includes both terms.

Although, strictly speaking, our asymptotic work was predicated upon the assumption $\mu^{1/6} \gg 1$, the accuracy of our approximations does not appear to be seriously hampered by this constraint. Our analysis has also yielded a two-term approximation for the so-called critical mode number (m_c), which predicts the number of equiangular spiral wrinkles localised near the upper rim; this formula corresponds to (4.3a) with M_0 and M_1 given by equations (4.7) and (7.7), respectively. Again, in terms of the physical variables

$$m_c = \delta_1(1-\nu^2)^{1/4}\cos\phi_0\left(\frac{R}{h}\right)^{1/2} + \delta_2(1-\nu^2)^{1/12}\cos\phi_0\tan^{2/3}\phi_0\left(\frac{R}{h}\right)^{1/6} + \dots, \qquad (8.2)$$

with $\delta_1 \simeq 1.1316$ and $\delta_2 \simeq 1.6947$.

An important simplification in the bifurcation equations discussed in this paper was directly linked to adopting the membrane solution (2.4) for the basic state. In light of the shallow geometries considered here this is a reasonable assumption. However, for larger values of the terminal latitude angle ϕ_0 (see Figure 2) one might have to account for geometrical nonlinearities prior to buckling, even though such effects might eventually turn out to be of little consequence to the overall picture that has transpired from the current investigation. As for the actual DMV bifurcation equations, since buckling takes place with a large number of circumferential wrinkles, these are likely to remain valid even for non-shallow shells; of course, the case $\phi_0 \to 90°$ will require a more delicate analysis of the corresponding bifurcation equations because the coefficients recorded in Appendix A exhibit singular behaviour in that limit.

It was mentioned in §1 that Mow and Sadowski [47] considered a situation somewhat related to our topic. However, as they dealt essentially with a complete hemisphere subjected to a *concentrated* polar twisting moment, there is no easy way to establish a direct parallel with our own findings (since

the equatorial region discussed herein is relatively far from the poles of the sphere). If only the critical torque is needed (i.e., the post-bifurcation regime is of no interest), one can use a shallow-shell approximation for a spherical cap to examine the behaviour of both λ_c and m_c by following a similar analysis as in this work. This might help elucidate the status of the ad-hoc treatment of [47] vis-à-vis the more established route pursued in this work.

Shallow hemispherical configurations akin to the one studied here are usually encountered in pressure vessels or as linking elements between pressurised pipes of different diameters [1, 29, 69]. In this context it would be of interest to consider the effect that an internal pressure might have on the critical torque responsible for the buckling instability. We note that this would amount to the first two terms in (2.4) becoming non-zero which, in turn, will add several other contributions to the original differential system (2.8); the structure of such extra terms can be gleaned from reference [12] (see equations (2.1) therein). In this case the pressure is expected to play a passive role and the final results will likely depend on the scaling of the pressure with μ. We hope to return to this problem in the near future.

We are grateful to the referees whose numerous comments helped improve the structure and the presentation of the key elements of the paper.

A Coefficients of the bifurcation equations

Here we record the definitions of the coefficients $\mathcal{A}_{ijk}$ that appears in the definitions of the operators $\mathcal{L}_{ij}$ that form the perturbation equations (2.8). In particular, in $\mathcal{L}_{11}$ and $\mathcal{L}_{12}$ we have

$$\mathcal{A}_{114} = 1\,,$$

$$\mathcal{A}_{113} = -2\tan\phi\,,$$

$$\mathcal{A}_{112} = -2(1+m^2)\sec^2\phi + \tan^2\phi\,, \qquad \mathcal{A}_{122} = -\mu^2\,,$$

$$\mathcal{A}_{111} = -(1+2m^2)\sec^2\phi\tan\phi + \mathrm{i}\lambda m\sec^3\phi\,, \qquad \mathcal{A}_{121} = \mu^2\tan\phi\,,$$

$$\mathcal{A}_{110} = m^2\sec^2\phi\left[(m^2-2)\sec^2\phi - 2\tan^2\phi\right] + \mathrm{i}\lambda m\sec^3\phi\tan\phi\,, \qquad \mathcal{A}_{120} = \mu^2 m^2\sec^2\phi\,,$$

The coefficients in $\mathcal{L}_{21}$ and $\mathcal{L}_{22}$ are

$$\mathcal{A}_{224} = 1\,,$$

$$\mathcal{A}_{223} = -2\tan\phi\,,$$

$$\mathcal{A}_{222} = -2(1+m^2)\sec^2\phi + \tan^2\phi\,, \qquad \mathcal{A}_{212} = 1\,,$$

$$\mathcal{A}_{221} = -(1+2m^2)\sec^2\phi\tan\phi\,, \qquad \mathcal{A}_{211} = -\tan\phi\,,$$

$$\mathcal{A}_{220} = m^2\sec^2\phi\left[(m^2-2)\sec^2\phi - 2\tan^2\phi\right]\,, \qquad \mathcal{A}_{210} = -m^2\sec^2\phi\,.$$

B Details of the solution for $f_0(X)$ and $g_0(X)$

Here we outline the procedure required to solve the system (5.5) for the functions $f_0(X)$ and $g_0(X)$. We can find five linearly independent solutions of this problem which do not grow exponentially; these are given by

$$(f_0, g_0) = (1, 1), \quad \left(X, X + \mathrm{i}\sqrt{2}\right), \quad (e^{p_4 X}, 0), \quad \left(X, \frac{\mathrm{i}}{\sqrt{2}}\right) e^{p_4 X} \quad \text{and} \quad (1, -1 + 2\mathrm{i}) e^{p_6 X},$$

where it is recalled that $p_4 = \dfrac{-1+\mathrm{i}}{\sqrt{2}}$ and $p_6 = \sqrt{2}(-1+\mathrm{i})$. We then choose the appropriate linear combination of these that fulfils the boundary conditions specified in (5.4), and this leads directly to the forms set out in the solutions (5.7).

References

[1] Bickell, M.B., Ruiz, C. : Pressure Vessel Design and Analysis. Macmillan Education, London (1967)

[2] Blum, R.E., McComb, H.G.: Buckling of an equatorial segment of a spherical shell loaded by its own weight. *Technical Note NASA-TN-D-4921* (1968)

[3] Blumenthal, O.: Über asymptotische Integration von Differentialgleichungen mit Anwendung auf die Berechnung von Spannungen in Kugelschalen. In : *Proceedings of the Fifth International Congress of Mathematicians, Vol. 2*, E.W. Hobson, A.E.H. Love (Eds.), 319–327. Cambridge University Press; Cambridge, 1913.

[4] Blumenthal, O.: Über asymptotische Integration von Differentialgleichungen mit Anwendung auf die Berechnung von Spannungen in Kugelschalen. Zeitschrift für Mathematik und Physik **62**, 343–358 (1914)

[5] Boyd, J.P.: Solving Transcendental Equations: The Chebyshev Polynomial Proxy and Other Numerical Rootfinders, Perturbation Series, and Oracles. Society for Industrial and Applied Mathematics, Philadelphia (2014)

[6] Bushnell, D.: Computerized Buckling Analysis of Shells. Kluwer Academic Publishers, Dordrecht (1989)

[7] Brush, Don O., Almroth, Bo O.: Buckling of Bars, Plates and Shells. McGraw-Hill Book Company, New York (1975)

[8] Cheng, H.: Advanced Analytic Methods in Applied Mathematics, Science, and Engineering. LuBan Press, Boston (2007)

[9] Collatz, L.: Eigenwertprobleme und ihre Numerische Behandlung. Chelsea Publishing Company, New York (1948)

[10] Coman, C.D.: Some applications of the WKB method to the wrinkling of bi-annular plates in tension. Acta Mech. **224**, 399–423 (2013)

[11] Coman, C.D.: Bifurcation instabilities in finite bending of circular cylindrical shells. International Journal of Engineering Science **119**, 249–264 (2017)

[12] Coman, C.D.: Tensile bifurcations in a truncated hemispherical thin elastic shell. Zeitschrift für Angewandte Mathematik und Physik **71:178** (2020)

[13] Coman, C.D., Bassom, A.P.: On the wrinkling of a pres-stressed annular thin film in tension. J. Mech. Phys. Solids **55**, 1601–1617 (2007)

[14] Coman, C.D., Bassom, A.P.: Boundary layers and stress concentration in the circular shearing of thin films. Proceedings of the Royal Society of London A **463**, 3037–3053 (2007)

[15] Coman, C.D., Bassom, A.P.: Wrinkling of pre-stressed annular thin films under azimuthal shearing. Mathematics and Mechanics of Solids **13**, 513–531 (2008)

[16] Coman, C.D., Matthews, M.T., Bassom, A.P.: Asymptotic phenomena in pressurised thin films. Proceedings of the Royal Society of London A **471**, 20150471 (2015)

[17] Coman, C.D., Bassom, A.P.: Asymptotic limits and wrinkling patterns in a pressurised shallow spherical cap. Int. J. Non-linear Mech. **81**, 8–18 (2016)

[18] Coman, C.D., Bassom, A.P.: On the role of in-plane compliance in edge wrinkling. Journal of Elasticity **126**, 135–154 (2017)

[19] Coman, C.D., Bassom, A.P.: Wrinkling structures at the rim of an initially stretched circular thin plate subjected to transverse pressure. SIAM Journal of Applied Mathematics **78**, 1009–1029 (2018)

[20] Coman, C.D., Haughton, D.M.: Localized wrinkling instabilities in radially stretched annular thin films. Acta Mech. **185**, 179–200 (2006)

[21] Du, Y., Sun, L. Li, S., Li, Y.: Vibration analysis of truncated spherical shells under various edge constraints. Thin-Walled Structures. **147**, 106544 (2020)

[22] Fedoryuk, M.V.: Asymptotic Analysis. Springer-Verlag, New York (1993)

[23] Feschenko, S.F., Shkil', N.I., Nikolenko, L.D.: Asymptotic Methods in the Theory of Linear Differential Equations. American Elsevier Company, New York (1967)

[24] Flügge, W.: Stresses in Shells (2nd ed.). Springer-Verlag, Berlin (1973)

[25] Fu, Y.B.: Some asymptotic results concerning the buckling of a spherical shell of arbitrary thickness. International Journal of Non-Linear Mechanics 33, 1111–1122 (1998)

[26] Fu, Y.B., Sanjarani Pour, M.: WKB method with repeated roots and its application to the buckling analysis of an everted cylindrical tube. SIAM Journal of Applied Mathematics **62**, 1856–1871 (2002)

[27] Geckler, J.W.: Über die Festigkeit achsensymmetrischer Schalen. Forschungsarbeiten auf dem Gebiete des Ingenieurwesens **276**, VDI-Verlag, Berlin (1926)

[28] Geckler, J.W.: Zur Theorie der Elastizität flacher rotationssymmetrischer Schalen. Ingenieur-Archiv **276**, 255–270 (1930)

[29] Gill, S.S. (ed.): The Stress Analysis of Pressure Vessels and Pressure Vessels Components Pergamon Press, Oxford (1970)

[30] Gould, S.H.: Variational Methods for Eigenvalue Problems. Dover Publications, New York (1995)

[31] Grigolyuk, E.I., Kabanov, V.V.: Stability of Shells (in Russian). Nauka, Moscow, (1978)

[32] Havers, A.: Asymptotische Biegetheorie der unbelasteten Kugelschale. Ingenieur-Archiv **6**, 282–312 (1935)

[33] van der Heijden, A.M.A.: W.T. Koiter's Elastic Stability and Structures. Cambridge University Press, Cambridge (2008)

[34] Hetenyi, M.: Spherical shells subjected to axial symmetrical bending. International Association for Bridge and Structural Engineering, Publication **5**, Zürich, 173–185 (1938)

[35] Hutchinson, J.W.: Knockdown factors for buckling of cylindrical and spherical shells subject to reduced bi-axial membrane stress. International Journalof Solids and Structures **47**, 1443–1448 (2010)

[36] Jawad, M.H.: Stress in ASME pressure vessels, boiler and nuclear components. John Wiley & Sons, New York (2018)

[37] Kalamkarov, A.L, Andrianov, I.I.: Analytical solution of the stability problem for the truncated hemispherical shell under tensile loading. Mathematical Problems in Engineering. **2018**, article ID: 5260639 (2018)

[38] Lagerstrom, P.A.: Matched Asymptotic Expansions: Ideas and Techniques. Springer-Verlag, New York (1988)

[39] Langer, R.E.: On the asymptotic solutions of ordinary differential equations with reference to the Stokes' phenomenon about a singular point. Transactions of the American Mathematical Society **37**, 397–416 (1935)

[40] Leckie, F.A.: Asymptotic solutions for the spherical shell subjected to axially symmetric loading. In : *Symposium on Nuclear Reactor Containment Buildings and Pressure Vessels*, The Royal College of Science and Technology, Glasgow, 286–297. Butterworths; London (1960)

[41] Leckie, F.A.: Localized loads applied to spherical shells. Journal of Mechanical Engineering Science **3**, 111–118 (1961)

[42] Li, H.: Free vibration of a high-speed rotating truncated spherical shell. Journal of Vibration and Acoustics **135**, 031006-1 (2013)

[43] Lin, C.C.: The Theory of Hydrodynamic Stability. Cambridge University Press, Cambridge (1955)

[44] Meissner, E.: Das Elastizitätsproblem dünner Schalen von Ringflächen, Kugel- oder Kegelform. Physikalische Zeitschrift **14**, 343–349 (1913)

[45] Meksyn, D.M.: New Methods in Laminar Boundary-Layer Theory. Pergamon Press, Oxford (1961)

[46] Mikulas, M.M.: Behaviour of a flat stretched membrane wrinkled by the rotation of an attached hub. *Technical Note NASA-TN-D-2456* (1964)

[47] Mow, C.C., Sadowski, M.A.: Determination of the critical torque inducing buckling in a twisted spherical shell subject to internal or external pressure. In: *Proceedings of Army Science Conference, U.S. Military Academy, West-Point,New York, 20-22 June 1962;* pp.129–139. Armed Services Technical Information Agency; Arlington, Virginia (1962)

[48] Mushtari, Kh.M., Galimov, K.Z.: Non-linear Theory of Thin Elastic Shells. Tatknigoizdat, Kazan, Russia (1957)

[49] Nayfeh, A.H., Mook, D.T.: Nonlinear Oscillations. John Wiley & Sons, Inc., New York (1979)

[50] Niordson, F.I.: Free vibrations of thin elastic spherical shells. International Journal of Solids and Structures **20**, 667–687 (1984)

[51] Niordson, F.I..: Shell Theory. North-Holland, Amsterdam (1985)

[52] Olver, F.W.J.: The asymptotic solution of linear differential equations of the second order for large values of a parameter and the asymptotic expansion of Bessel functions of large order. Philosophical Transactions of the Royal Society of London, A **247**, 307–327 (1954)

[53] Pedersen, P.T., Jensen, J.J.: Buckling of spherical cargo tanks for liquid natural gas. Royal Institution of Naval Architects, Transactions **118**, 193–205 (1976)

[54] Pedersen, P.T., Jensen, J.J.: Buckling behaviour of imperfect spherical shells subjected to different load conditions. Thin-Walled Structures **23**, 41–55 (1995)

[55] Pogorelov, A.V.: Geometric Theory of Shell Stability (in Russian). Nauka, Moscow (1966)

[56] Pogorelov, A.V.: Bendings of Surfaces and Stability of Shells. American Mathematical Society, Providence, Rhode Island (1988)

[57] Reissner, E.: On tension field theory. In: *Proceedings of the 5th International Congress of Applied Mechanics*, J.P. Den Hartog, H. Peters (Eds.), 88–92. John Wiley & Sons; New York, 1939.

[58] Reissner, E.: On axisymmetric deformations of thin shells of revolution. In: *Proceedings of the Third Symposium in Applied Mathematics. Vol III: Elasticity*, R.V. Churchill, E. Reissner, A.H. Taub (Eds.), 27–52. McGraw-Hill Company, New York (1950)

[59] Reissner, H.J.: Spannungen in Kugelschalen (Kuppeln). In: *H. Müller-Breslau Festschrift*, pp. 181–193. A. Kröner, Leipzig, 1912.

[60] Sanders, J.L. Jr.: Nonlinear theories for thin shells. Quart. Appl. Math. **6**, 21–36 (1963)

[61] Sano, A., Izumi, N., Matsubara, N., Fujikubo, M.: Estimation of elastic buckling strength of a non-spherical tank in the partially filled condition. In: *Proceedings of the ASME 2017 36th International Conference on Ocean, Offshore and Arctic Engineering OMAE2017: June 25-30 2017, Trondheim, Norway.* OMAE2017-61397. American Society of Mechanical Engineers, New York (2017)

[62] Singer, J., Arbocz, J., Weller, T.: Buckling Experiments (Vol. 2). John Wiley & Sons, New York (2002)

[63] Singh, A.V., Mirza, S.: Asymmetric modes and associated eigenvalues for spherical shells. J. Pressure Vessel Technol. **107**, 77–82 (1985)

[64] Steele, C.R.: Application of the WKB method in solid mechanics. In: *Mechanics Today, Vol. 3*, S. Nemat-Nasser (Ed.), 243–295. Pergamon Press, New York (1976)

[65] Tall, M., Hariri, S., Le Grognec, P., Simonet, Y.: Elastoplastic buckling and collapse of spherical shells under combined loadings. Thin-Walled Structures **123**, 114–125 (2018)

[66] Tovstik, P.E., Smirnov, A.L.: Asymptotic Methods in the Buckling of Elastic Shells. World Scientific Publishing, Singapore (2001)

[67] Troger, H., Steindl, A.: Nonlinear Stability and Bifurcation Theory. Springer-Verlag, Wien (1991)

[68] Ventsel, E., Krauthammer, T.: Thin Plates and Shells: Theory, Analysis, and Applications. Marcel Dekker, Inc., New York (2001)

[69] Vlasov, W.S.: Allgemeine Schalentheories und ihre Anwendung der Technik. Akademie-Verlag, Berlin (1958)

[70] Wasow, W.: Asymptotic Expansions for Ordinary Differential Equations. Interscience Publishers, New York (1965)

[71] Yao, J.C.: Buckling of a truncated hemisphere under axial tension. AIAA Journal **1**, 2316-2319 (1963)

[72] Yiniy, Z.: Torsional buckling of spherical shells under circumferential shear loads. Applied Mathematics and Mechanics **20**, 426–432 (1999)

[73] Zingoni, A.: Shell Structures in Civil and Mechanical Engineering: Theory and Analysis (2nd ed.). ICE Publishing, New York (2017)